The Astrophysical Journal, 738:14 (7pp), 2011 September 1 doi:10.1088/0004-637X/738/1/14

LUNAR DUST GRAIN CHARGING BY ELECTRON IMPACT: DEPENDENCE OF THE SURFACE POTENTIAL ON THE GRAIN SIZE

Z. Němeček[1], J. Pavlů[1], J. Šafránková[1], M. Beránek[1], I. Richterová[1], J. Vaverka[1], and I. Mann[2]
[1] Faculty of Mathematics and Physics, Charles University, Prague, Czech Republic
[2] Belgian Institute for Space Aeronomy, Brussels, Belgium
Received 2011 February 17; accepted 2011 June 5; published 2011 August 9

ABSTRACT

The secondary electron emission is believed to play an important role for the dust charging at and close to the lunar surface. However, our knowledge of emission properties of the dust results from model calculations and rather rare laboratory investigations. The present paper reports laboratory measurements of the surface potential on Lunar Highlands Type regolith simulants with sizes between 0.3 and 3 μm in an electron beam with energy below 700 eV. This investigation is focused on a low-energy part, i.e., $\leqslant$100 eV. We found that the equilibrium surface potential of this simulant does not depend on the grain size in our ranges of grain dimensions and the beam energies, however, it is a function of the primary electron beam energy. The measurements are confirmed by the results of the simulation model of the secondary emission from the spherical samples. Finally, we compare our results with those obtained in laboratory experiments as well as those inferred from in situ observations.

Key words: dust, extinction – planetary systems

1. INTRODUCTION

Photoelectron emission, sticking and recombination of plasma particles, secondary electron emission (SEE), thermionic and field ion and electron emissions electrically charge dust grains in space. Their charge depends on the UV flux, the size, shape, and structure of the grains, their velocity relative to the plasma, and the plasma temperature. Since photoelectron, secondary electron, and thermionic emissions vary with the material, the dust surface charge is also influenced by the dust composition. As a result of the dominating photoelectron emission caused by the solar radiation, dust grains in the interplanetary medium are usually positively charged and their charges correspond to surface potentials relative to infinity between 5 and 10 V (Mukai 1981; Whipple 1981). Differences among dust grains of various compositions occur for higher plasma temperatures where SEE becomes important (Kimura & Mann 1998). Moreover, the dust surface potential depends on the charging history of grains (Whipple 1981; Meyer-Vernet 1982; Velyhan et al. 2004).

In the space, grain charging by SEE due to the impact of energetic electrons is significant in environments where these high-energy electrons are present. In dense plasma regions where the electron flux is significant, the sign and value of the dust grain surface potential are determined by the energy of the impinging electrons. Electron attachment dominates in the eV range but, at electron energies above about 10 eV, SEE becomes important and causes a reduction of the negative potential. When the total SEE yield reaches the value larger than unity, the surface potential changes its sign from negative to positive values (Meyer-Vernet 1982; Horanyi & Goertz 1990). This effect has been demonstrated in laboratory experiments (Walch et al. 1998; Pavlů et al. 2009).

Richterová et al. (2007) have studied the profiles of equilibrium surface potentials at glass grains as a function of the beam energy over a wide range of diameters. The low-energy parts (below several hundreds of eV) of the profiles are identical because neither η (the backscattered yield defined as the mean number of backscattered electrons per one primary electron) nor δ (the secondary electron yield) depend on the grain diameter in this energy range. The shape of these parts of the curves is determined by the energetic dependence of the secondary emission yield and energy spectrum of secondary electrons. This approach was applied, for instance, to the charging of water ice grains in the Saturn magnetosphere, where Jurac et al. (1995) show that the surface potentials are not sensitive to the grain size as long as the grains are not much smaller than 0.1 μm.

On the other hand, high-energy parts strongly depend on the grain size. This effect is connected with an increasing number of backscattered primary electrons. When η approaches unity, the grain is charged positively by outgoing secondary electrons because primary electrons do not compensate this charge and the potential of the grain rises.

The lunar surface is composed of rocks and regolith, i.e., soil-like layer with the grain size from centimeters to submicron scales (e.g., Stubbs et al. 2006). The surface is exposed to solar ultraviolet (UV) and X-rays as well as solar and magnetospheric plasma and energetic particles (Halekas et al. 2009b). All these processes generate currents to the surface and can produce an escaping flux of secondary electrons. Each of these charging currents depends on the electrostatic potential of the surface with respect to the surrounding plasma. Due to high variability of these charging currents along the Moon orbit around the Earth, lunar surface potentials can vary over orders of magnitude (Halekas et al. 2005, 2007). On the sunlit hemisphere of the Moon, photoelectron currents usually prevail, and the surface charges to a small positive potential. On the night side, currents of energetic electrons tend to dominate, and the surface charges to a negative potential. However, SEE can complicate expectations providing an additional positive current source, and thus the nightside surface could even charge positive (Halekas et al. 2008). Evaluation of the Lunar Prospector (Halekas et al. 2009a) in situ measurements suggests that the secondary emission yield of the lunar regolith is by a factor $\approx$3 lower than the measured for samples in the laboratory. By contrast, Abbas et al. (2010) reported laboratory results of the charging of dust grains with dimensions of 0.2–13 μm selected from the Apollo 11 and 17 missions and exposed by the monoenergetic electron beam in the 10–200 eV energy range. The authors obtained much larger secondary emission yield than reported

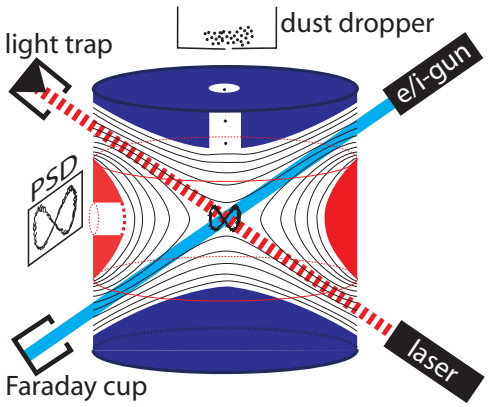

Figure 1. Principles of the experimental setup. The AC voltage is applied between blue and red rotationally symmetric hyperbolic electrodes; the thin black lines stand for its equipotentials. The grain oscillations are projected onto the position sensitive detector (PSD). Note that the frequency in the radial direction is twice large than in the axial direction due to the geometry of our trap.

from other laboratory investigations (e.g., Richterová et al. 2007).

The lunar regolith consists of dust grains of various sizes, and the distant spacecraft cannot resolve individual potentials but provides a mean value. As noted above, it is generally expected and proved by secondary emission models that the grain potential depends on the incident electron energy but not on the dimensions of individual grains. Consequently, the measured mean value would be about equal to the surface potentials of individual grains on or above the lunar surface. However, Abbas et al. (2010) estimations provide the equilibrium surface potential independent on the primary energy but rising with the grain size.

Uncertainties in secondary emission yield estimations may contribute to the poor accuracy of predictions from models, thus new laboratory measurements of the secondary emission from a lunar regolith under realistic charging conditions could solve this issue. For this reason, we studied changes of the surface potential of small grains (with sizes of 0.3–3 μm) in a narrow energy range (75 and 100 V) because it is a lower limit of our apparatus (and our electron beam source). We used Lunar Highlands Type (LHT) lunar stimulant, thus we can directly compare our results with measurements of other authors or with in situ observations.

2. EXPERIMENTAL SETUP

The heart of our measuring setup is schematically shown in Figure 1. Since details of our experiment can be found in Čermák (1994), Čermák et al. (1995), Žilavý et al. (1998), and Pavlů et al. (2004b, 2009), we will describe only the principal features for the present paper.

Our investigations are based on trapping a single dust grain in an electrodynamic quadrupole and its influencing by tunable monoenergetic ion and/or electron beams. The quadrupole is supplied with the symmetrical AC voltage (the voltage ranges usually from 400 to 900 V in a frequency range of 0.3–3 kHz), thus the zero potential is in the middle of the trap where the grain is levitating. Moreover, this configuration provides a straight line through the trap along which the AC potential is zero (Figure 1). Consequently, the energy of the beam firing along this line is not altered.

From the quadrupole theory it follows that the vertical electrodes should be supplied by the same voltage. However, we are using two different amplifiers for them in order to apply a symmetrical dumping voltage and symmetrical DC voltage for the compensation of the gravity force. These voltages are small (several volts) but they can deflect the electron beam. Moreover, the AC electric field perpendicular to the beam direction deflects this electron beam. For these reasons, both the electron gun and quadrupole power supply are equipped with a sampling electronics. The electron beam is switched on only inside the time window when the quadrupole voltage is pulled down to zero. According to the test, switching off the quadrupole voltage up to 1/10 of the period does not measurably change the frequency of grain oscillations (Žilavý et al. 1998; Pavlů et al. 2009).

A trapped grain is irradiated by a 635 nm diode laser modulated by 10 kHz. The light scattered by the grain passes a small window in the ring electrode (electrically screened by a grid) and is collected by a simple lens system. The magnified grain image is projected onto the entrance of an image intensifier and its output is optically coupled to a position sensitive detector. Signals from this coordinate detector are amplified by narrow band, and lock-in amplifiers prior to the coordinates of the light spot are calculated. These coordinates are used to control the grain motion by the damping system and to determine the grain oscillation frequency (in the axial direction in our particular case) by a counter or by Fourier analysis.

After several simplifications, theoretical considerations (Čermák 1994) lead to the following relation between the grain oscillation frequency and its charge-to-mass ratio (specific charge, Q/m):

$$\frac{|Q|}{m} = \pi^2 r_0^2 \cdot \frac{f_{\mathrm{AC}} \cdot f}{V_{\mathrm{eff}}} \cdot \frac{1}{\sqrt{1 + (1.8 f / f_{\mathrm{AC}})^2}}, \qquad (1)$$

where $V_{\mathrm{eff}} = V_{\mathrm{AC}}/\sqrt{2}$ is the rms value of the AC voltage on the quadrupole electrodes, V_{AC} is its amplitude, f_{AC} is the frequency of the applied AC voltage, f is the frequency of the grain oscillation in the axial direction, and r_0 denotes the inner radius of the quadrupole ring electrode ($r_0 = 10$ mm).

This relation is based on the assumption of an adiabatic motion of the grain in the quadrupole field. This is valid for a sufficiently high ratio between frequencies of the applied AC voltage and of grain oscillations. Further, the expression assumes an ideal quadrupole field. Any deviation from the ideal hyperbolic geometry results in a contribution of higher multipoles to the total field, the effective potential is non-harmonic and the grain oscillation frequency becomes amplitude dependent. Since the deviation from the quadrupole field increases with the oscillation amplitude, the amplitude must not exceed a certain value for a desired accuracy of the frequency determination. Therefore, a damping system keeps the oscillation amplitude constant at the reasonable level.

The experiment can be run in a broad range of pressures but special techniques were used to allow the operation under ultrahigh vacuum conditions (10^{-9} torr). This is essential in order to reduce the interaction of the grain surface with molecules of the residual atmosphere and to decrease the grain charging by products of ionization of the residual gas. Assuming the pressure of 10^{-9} torr, the mean free path of electrons is of the order of 10^6 cm. Since the ratio of the beam and grain cross-sections is similar, we can expect that the number of ionization events and the number of beam electrons striking

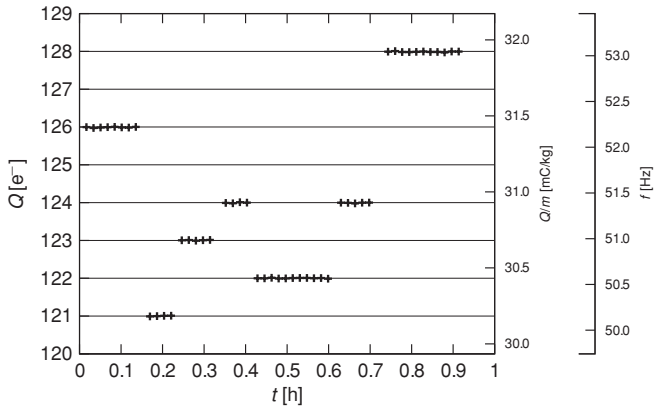

Figure 2. Determination of the grain mass by the elementary charge method. The grain mass calculated from frequency jumps is 6.44×10^{-16} kg.

the grain surface are also similar. The direction of motion of the ionization products is arbitrary and thus their contribution to the grain charging is negligible.

The grain oscillation frequency is the only measurable quantity, and we have developed several techniques to determine the grain mass, charge, capacitance, and surface potential. The detailed description of these techniques can be found in above-mentioned papers, thus we only briefly comment on them here.

The specific charge (charge-to-mass ratio) is determined from the grain oscillation frequency using Equation (1). The charge and mass are separated by a method analogous to the Millikan experiment (Žilavý et al. 1998). A procedure is as follows: the grain is charged by a small (up to several hundreds) number of electrons to be reliably trapped. Then, its charge is changed by a few electrons and the variances of its oscillation frequency together with the known elementary charge allow us to determine the grain mass. We used a low-energy electron beam with a minimum possible intensity, a duration of the sampling pulse ≈1 ms and with a repetition period of ≈6 minutes. Figure 2 shows an example of such measurements. There are three scales on the vertical axis—the measured oscillation frequency of the grain, f in the axial direction, the values of the Q/m ratio calculated according to Equation (1) (two right-hand scales), and the grain charge in units of the elementary charge (the left axis) that was obtained by the linear regression of the data that assigned the steps to the number of electrons (Žilavý et al. 1998; Pavlů et al. 2009). Note that the grain charge steps up and down because the yield of the secondary emission is close to unity for the chosen beam energy, thus impacts of individual electrons can result in both decreasing or increasing of the grain charge due to statistical nature of the emission process. The error of the mass determination depends on many factors but it does not exceed ≈1% under conditions discussed in the present paper.

The grain charge is connected with its surface potential via grain capacitance. To determine it, the grain is charged to a high positive potential by the beam of Ar^+ ions. Then, the energy of the beam is decreased and the beam Ar ions cannot impact the grain but they are scattered in the grain electric field and interact with the residual gas and quadrupole electrodes. These interactions produce low-energy electrons that are attracted by the positive grain, thus the grain is gradually discharged. After some time (≈2 hr), the grain potential becomes numerically equal to the beam energy and the current of beam electrons starts to compensate discharging current. Since both currents are

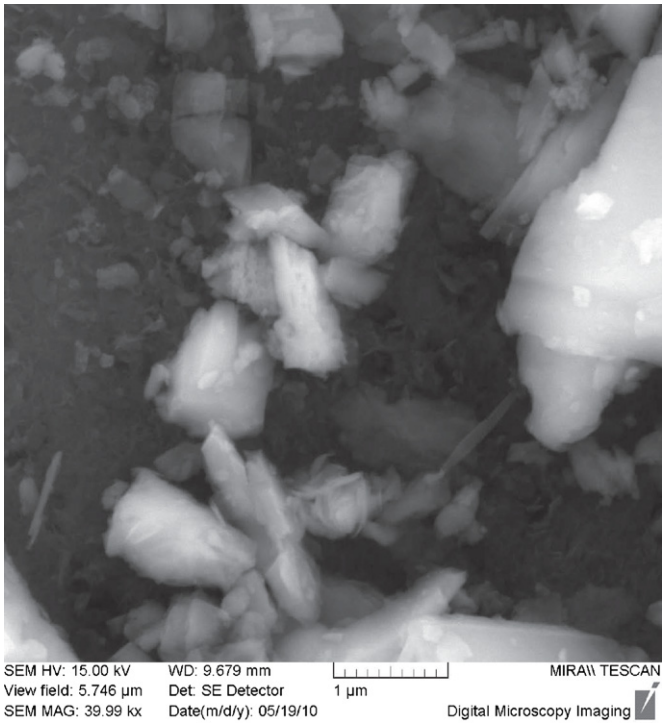

Figure 3. SEM photo of LHT analogs.

linear functions of the grain charge, the point where the beam energy becomes equal to the grain potential can be easily found in the plot of Q/m versus time. This point allows us to determine the proportionality constant between the grain specific charge, Q/m and its surface potential, ϕ, i.e., the specific capacitance, C/m. The error of this method is larger than that for the mass determination. We will provide error estimations for each measurement of a particular grain, however, this error is lower than 10% in general.

3. EXPERIMENTAL RESULTS

The measurements were carried out on LHT dust analogs. The dust sample was produced by grinding from larger pieces, thus the shapes of individual grains are irregular as it can be seen from the scanning electron micrograph (SEM) photo in Figure 3.

Each grain was investigated in several steps that guarantee the same charging conditions and history for each of them.

1. The fresh dust grain was released from the dust dropper and bombarded by the ≈300 eV electron beam when falling through the quadrupole center. This procedure results in a positive charge that allows us the grain trapping.
2. The grain mass (and charge) was determined as described in the previous section.
3. The grain was charged by the electron beam of a tunable energy, and the equilibrium charge-to-mass ratio was recorded for each energy step.
4. The Ar^+ ion bombardment was used for determination of the grain capacitance (see above).
5. Using the known mass and capacitance, the grain specific charge was recalculated into the surface potential.

Figure 4 shows an example of the dependence of the grain surface potential on the beam energy. The paper is focused on lowest energies, but we are showing the measurements up to

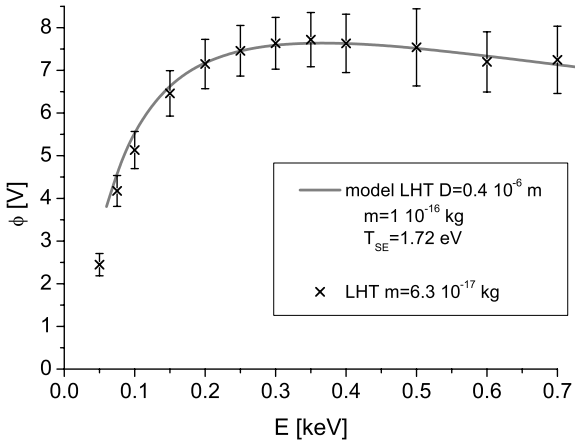

Figure 4. Dependence of the equilibrium surface potential on the energy of the primary electron beam. The crosses show the experimental data, and the full line presents the model prediction (Richterová et al. 2010).

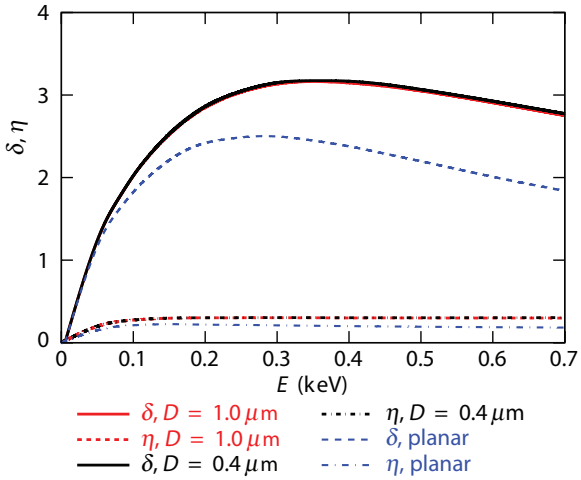

Figure 5. Modeled yields of the true, δ and backscattered, η secondary electrons for LHT spheres with 0.4 and 1 μm diameters. The dotted lines represent the same yields for a planar LHT sample.

700 eV. We are comparing experimental data with the results of the secondary emission model (Richterová et al. 2010). As it can be seen from the figure, the model describes the surface potential rather well at energies above 200 eV and slightly overestimated the potential at lower beam energies. Nevertheless, the differences between measured and modeled potentials stay within the range of measuring errors, thus the model prediction can be used as a support for interpretation of experimental data.

The electrons leaving the grain can be divided into two groups. The first of them, so-called backscattered electrons, consists of primary electrons that entered the grain, lost a part of their energy in the interaction with the grain atoms, and left the grain again. The ratio of numbers of these and all primary electrons is named the backscattered yield, η and cannot exceed unity. However, some electrons of the grain matter gain a sufficient energy to leave the grain in the interactions. Such electrons are called true secondary electrons and their yield, δ can vary in a broad range with the grain material, shape, and dimensions and with the primary electron beam.

The yield of the secondary emission cannot be measured directly but it can be considered as a scaling factor for the secondary emission model. Figure 5 shows the yield of the true

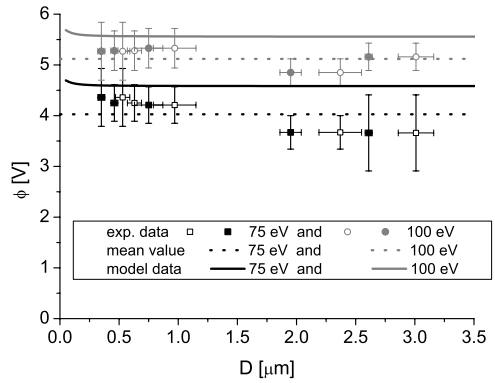

Figure 6. Dependencies of the equilibrium surface potential on grain sizes for two energies of the primary electron beam: 75 eV (squares) and 100 eV (circles). The open symbols stand for diameters determined from the grain capacitance, the filled symbols show the diameters estimated from the grain mass. The full lines show the results of the Richterová et al. (2010) model, and the dashed lines represent the mean values.

(δ) and backscattered (η) secondary electrons calculated for two LHT spheres (0.4 and 1 μm in diameter). For comparison, the calculations for a planar sample from the same material are shown as dotted lines in the figure. The corresponding profiles for two spheres cannot be distinguished in the figure, however, the differences between the planar sample and spheres are significant. This effect is known and is caused by an angular dependence of the secondary emission yield (Jurac et al. 1995; Richterová et al. 2010).

The experimental procedure described above is time consuming, thus we have a full set of measurements only for five grains of sufficiently different masses. The shape of a particular grain is unknown; we use the mass density given by the supplier—Zybek company (2900 kg m^{-3})—and calculate the grain effective diameter, D_m in a spherical approximation. This diameter can be compared with the value of D_C that was obtained from the grain capacitance; again in the spherical approximation. The measured mass, m, the capacitance, C, the diameters computed from these quantities, and their ratio, D_m/D_C, are given in Table 1 for all investigated grains. As it can be seen from the table, the D_m/D_C ratio varies in a broad range. Since the capacitance of the sphere is lower than the capacitance of any other object of the same volume (mass), the D_m/D_C ratio is close to unity for spherical objects, whereas deviation from unity suggests a more complicated shape.

The last two columns in Table 1 show the equilibrium potentials of grains measured under bombardment with the monoenergetic electron beam with the energy of 75 eV and 100 eV, respectively. Unfortunately, our present setup does not allow reliable measurements at lower energies.

The potentials from the table are plotted in Figure 6 as a function of the grain diameter. Since there are two different estimations of the grain diameter in Table 1, each measured point appears twice in Figure 6; at the positions corresponding to D_m and D_C. The dashed lines stand for the mean values of the measured potential for each energy. The full lines show the results of the Richterová et al. (2010) model. The model predicts a constant grain potential in the range from 0.2 to 3.5 μm of the grain diameter and a small rise of this potential for smaller grains. Taking into account the model prediction and the fact that a constant value fits to all measured data if the measuring error is considered, we can conclude that the surface potential is a rising function of the beam energy but it does not depend

Table 1
Details of Five Picked Grains

m (kg)	C (F)	D_m (μm)	D_C (μm)	D_m/D_C	ϕ_{75} (V)	ϕ_{100} (V)
$(6.4 \pm 1.1) \times 10^{-16}$	$(5.0 \pm 1.1) \times 10^{-17}$	(0.75 ± 0.12)	(0.97 ± 0.18)	(0.8 ± 0.3)	(4.2 ± 0.4)	(5.3 ± 0.4)
$(2.69 \pm 0.04) \times 10^{-14}$	$(1.68 \pm 0.08) \times 10^{-16}$	(2.61 ± 0.03)	(3.01 ± 0.15)	(0.87 ± 0.05)	(3.7 ± 0.8)	(5.2 ± 0.3)
$(1.12 \pm 0.05) \times 10^{-14}$	$(1.3 \pm 0.1) \times 10^{-16}$	(1.95 ± 0.09)	(2.37 ± 0.18)	(0.82 ± 0.10)	(3.7 ± 0.3)	(4.9 ± 0.3)
$(1.44 \pm 0.08) \times 10^{-16}$	$(3.5 \pm 0.3) \times 10^{-17}$	(0.46 ± 0.03)	(0.63 ± 0.06)	(0.73 ± 0.12)	(4.3 ± 0.4)	(5.3 ± 0.4)
$(6.6 \pm 0.5) \times 10^{-17}$	$(2.9 \pm 0.4) \times 10^{-17}$	(0.35 ± 0.03)	(0.53 ± 0.06)	(0.66 ± 0.13)	(4.4 ± 0.6)	(5.3 ± 0.6)

Notes. m is a measured mass of the grain, C is a measured capacitance, D_m and D_C are estimated effective diameters based on measured mass and capacitance, respectively, ϕ_{75} and ϕ_{100} are calculated equilibrium surface potentials of a particular grain under 75 eV and 100 eV electron bombardment, respectively. The errors represent three standard deviations.

on the grain mass in the investigated energy range. The slight decrease of the grain potential with the grain size for 75 V of the beam energy is in the range of measuring errors. Moreover, we can note that the equilibrium potential does not depend on the grain shape because the shape parameter, D_m/D_C varies over a broad range (Table 1).

4. DISCUSSION OF RESULTS

Our measurements show that the equilibrium potential of the grain illuminated by the low-energy (75–100 eV) parallel electron beam does not depend on the grain dimensions and shapes but that it is a rising function of the energy. This is consistent with our previous investigations of the secondary emission from dust grains of different materials (e.g., Richterová et al. 2004, 2006; Pavlů et al. 2008, 2009). These experimental investigations revealed that the effects of shape would be notable either for very small (tens of nanometers) grains or for grain dimensions in the micrometer range with energies exceeding $\approx$1 keV. The same conclusion follows from model calculations (Jurac et al. 1995; Richterová et al. 2010).

Fitting of our measurements to the model leads to the secondary emission yield $\delta \approx 2$ at 100 eV and $\delta \ll 1$ at 10 eV of the primary beam energies. As it can be seen in Figures 4 and 6, the model overestimates the potentials at the low primary energies. There can be two reasons for this overestimation: (1) the distribution of true secondary electrons is non-Maxwellian or (2) the real yield of secondary emission is lower than that given by the model in this range of energies.

Our estimations lead to the maximum of the secondary emission yield $\delta \approx 3.2$ (at about 350 eV) for a small dust grain. This is consistent with previous laboratory experiments but it is much larger than that follows from the Halekas et al. (2009a) analysis of in situ observations. We believe that the value of δ for a planar surface would be more appropriate to the interpretation of the data measured at larger distances from the lunar surface because it reflects partly the effects of a surface roughness. Nevertheless, this value is still larger than an integral value suggested by Halekas et al. (2009a).

On the other hand, Abbas et al. (2010) reported experimental investigations of the samples of the lunar dust and have shown the potential rising with the grain diameter but (as it can be deduced from the text) independent of the beam energy in similar ranges of the beam energies and grain dimensions and that a secondary emission yield varying from 3 to 5.4 at 10 eV of the primary energy.

The differences between our and Abbas et al. (2010) measurements are (1) we use the LHT lunar dust analog, whereas Abbas et al. (2010) investigated the real lunar dust; and (2) the measuring techniques are slightly different. Horányi et al. (1998) compared the secondary emission from two lunar dust stimulants (MLS-1 and JSC-1) and Apollo 17 soil sample in the energy range from 20 to 90 eV and they did not find any significant differences. Consequently, we do not expect that the difference between our and Abbas et al. (2010) results can be connected with different samples.

Let us discuss the energy balance of the secondary emission process. The primary electron is accelerated in the electric field of the charged grain and falls on the surface where it receives an additional energy equal to the work function of the grain material. The energy of the primary electron is then distributed among the electrons of the grain. Those electrons that gained the sufficient energy to overcome the surface barrier (represented by the work function) and grain surface potential leave the grain as secondary electrons. Figure 4 of Abbas et al. (2010) provides the following data: primary electron energy 10 eV, secondary emission yield 5.3, and surface potential 2.2 V. A typical work function of insulators can be considered as 5 eV (e.g., Sternovsky et al. 2001). The 10 eV electron is accelerated to 12.2 eV and receives additional 5 eV of the energy at the surface. The total energy is 17.2 eV. To leave the grain, a secondary electron should gain about 7.2 eV (it is a sum of the work function and the energy corresponding to the grain potential). Neglecting all energy losses, the secondary emission yield cannot exceed a value of $17.2/7.2 = 2.4$. We can conclude that the yield of 5.3 given in Abbas et al. (2010) contradicts to energy conservation.

From this short discussion, it is clear that the results in Figure 4(d) of Abbas et al. (2010) are based on a wrong interpretation of measurements in their Figure 4(c) and that some important factor(s) is(are) neglected. After a careful examination of the conditions of our and Abbas et al. (2010) experiments, we have identified three principal factors that can influence the interpretation of experimental results: (1) the effect of the quadrupole AC electric field on the energy distribution of the primary electrons, (2) influence of the residual gas in the quadrupole, and (3) the method of determining the mass/size of the grains. Thus, following three subsections address these points.

4.1. Quadrupole AC Electric Field and Energy Distributions of Primary Electrons

The Abbas et al. (2010) experiment is based on the trapping of a single dust grain inside the quadrupole-like trap that consists of upper and lower spherical cups and a ring electrode. Unfortunately, an important information on the design of the trap, frequency, and amplitude of the AC voltage applied on the ring electrode as well as the DC voltage used for charge measurements cannot be found neither in the article nor in given references (i.e., Spann et al. 2001; Abbas et al. 2002,

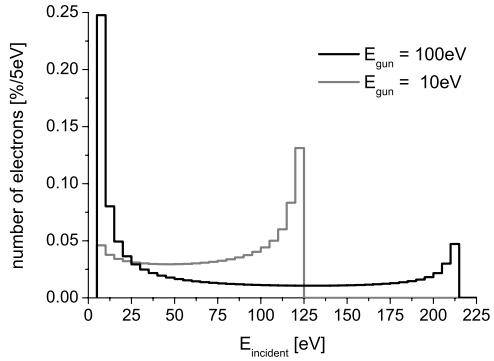

Figure 7. Distribution of electrons launched with the energies of 10 eV (gray) and 100 eV (black), respectively, on the 1 μm grain. The amplitude of the AC voltage is 500 V and geometry of the used model is described in the text. The simulation was performed using the SIMION® software package.

2004; Tankosic & Abbas 2008), thus the discussion is based on the information found in the mentioned papers and on our best estimates.

The electrons enter the trap along its vertical axis and they are influenced by the electric field resulting from the quadrupole AC voltage supplied to the ring electrode. We have used the geometry described in Spann et al. (2001) and modeled the trajectories of electrons within such trap. The amplitude of the AC voltage is 500 V and the top and bottom electrodes are grounded in our model. The electrons were launched from a spot of 1 mm in diameter at the center of the top electrode and the differential flux of electrons on a 1 μm grain placed in the trap center was recorded. Figure 7 shows the energy distribution of electrons launched with energies 10 and 100 eV, respectively. When the AC voltage is negative, primary electrons are decelerated and their energy decreases. Moreover, the negative ring electrode serves as a focusing electrostatic lens and increases the flux of electrons that fall onto the grain. On the other hand, the defocusing effect of the positive voltage decreases the primary flux and (at the same time) accelerates the electrons. It means that the grain is bombarded by electrons over a broad spectrum of energies.

The actual energies of impinging electrons depend on the trap geometry and the AC voltage, thus Figure 7 serves only as an example. Nevertheless, it is clear that considerations made in Abbas et al. (2010) that are based on the knowledge of the primary beam energy are not substantiated.

Moreover, if the numbers used in our model are realistic, the resulting spectrum of electrons launched with the energy of 10 eV will peak at ≈125 eV, whereas a much higher flux of 10 eV electrons will reach the grain when the electrons are launched with the energy of 100 eV. It could explain why Abbas et al. (2010) found a larger secondary emission yield for 10 eV than for 100 eV of the primary energy.

4.2. Influence of the Residual Gas Pressure

Figure 4(c) of Abbas et al. (2010) shows that the positive charge of the grain increases with time. The positive charging can be caused either by electrons leaving the grain or by positive ions falling onto it. Our Figure 7 demonstrates that even in the case of 10 eV primary electrons, the portion of energetic electrons is large enough to cause the SEE and thus it can be a source of the charging current. On the other hand, the energies of primary electrons are sufficient for ionization of the residual gas inside the trap. Moreover, the primary electrons are partly scattered in collisions with the molecules out of the trap axis and accelerated in the AC field to energies even higher than those shown in Figure 7. Since the mean free path of electrons is of the order of 10 m under experimental conditions of Abbas et al. (2010; pressure 10^{-5} to 10^{-6} torr), the ratio of the numbers of primary electrons falling on the grain and electrons colliding with the molecules of the residual gas would be $\approx 10^{-3}$. These collisions create electrons and positive or negative ions that can in turn alter the grain charge. The exact evaluation of the processes in the trap is impossible because the ongoing processes are complex and the boundary conditions are unknown. However, we would like to point out that the influence of the residual gas on the grain charging (especially to negative potentials) was investigated in Pavlů et al. (2004a) and it was shown (in their Figure 2) that the ion contribution should be considered even for pressures of the order of 10^{-8} torr under similar experimental conditions. We can suggest that aforementioned changes of the grain charge are connected with the contribution of the ion current rather than with variations of the secondary emission yield.

4.3. Determination of the Grain Mass and Potential

The mass of investigated lunar dust grains varies in a broad range but the methods of determination of the grain charge is based on knowledge of the mass of the particular grain. Our technique of the elementary charge (Figure 2) provides the grain mass with an uncertainty of the order of 1%.

The authors of Abbas et al. (2010) used the "spring-point method" (Davis 1985; Spann et al. 2001; Abbas et al. 2004; Tankosic & Abbas 2008, and references therein) that is based on a balance between the drag force and "heating" of the grain by the AC electric field in the quadrupole. However, the drag force strongly depends on the grain shape that is unknown. The authors of Abbas et al. (2010) apply a spherical approximation. They use the viscosity of the surrounding gas and experimental corrections that are based on the measurements with the spheres of known diameters. However, depending on the actual grain shape and direction of its motion, the drag coefficient can differ by an order of magnitude. Typical values of the drag coefficients are 0.42 for a sphere, 0.8–1.4 for a cube (depending on spatial orientation), and 2 for a plate perpendicular to the gas flow (e.g., Loth 2008). Neglecting the shape effect leads to overestimating the grain dimensions. For example, twice larger drag coefficient results in an overestimation of the effective diameter of the grain by a factor of $\sqrt{2}$. Since this diameter is used for an estimation of the grain mass, it would differ by a factor of ≈3 and the same uncertainty would apply to the determination of the grain charge.

Taking into account the experimental conditions inside the trap (pressure 10^{-3} torr), the molecular regime would be more appropriate for the drag force estimation because the mean free path of molecules is much larger than the characteristic dimensions of the grain. The exact calculations of the drag force is difficult but it can be simply shown (e.g., Dahneke 1973) that the drag exerting on a sphere and on a cylinder of the same volume (and mass) and twice larger diameter differ by a factor exceeding two and the consequences for the determination of the grain mass would be the same as in the case of viscous interaction discussed above.

5. CONCLUSION

We report the results of the measurements of the secondary emission yield and surface potential carried out on dust samples

from LHT lunar regolith simulants with sizes between 0.3 and 3 μm. We focused on an electron beam with energy below 700 eV. The interpretation of experimental results is supported by the computer model of the secondary emission from spherical samples that reflects the LHT mass composition. The conclusions listed below are different from those that Abbas et al. (2010) derived from their laboratory experiment and we point out some of physical inconsistencies in their data interpretation.

We can briefly summarize our investigations as follows.

1. The secondary emission yield rises with the primary beam energy up to a maximum of ≈3 at 350 eV (Figure 5).
2. The surface potential follows the increase of the secondary emission yield with the primary energy (Figure 4).
3. The surface potential does not depend on the dust grain mass, shape, and dimensions for the grains larger than 0.3 μm (effective diameter) and electron energies lower than ≈200 eV (Figure 6).

Finally, we would like to note that in our experiment, determined secondary emission yield is larger than that inferred from Lunar Prospector measurements above the lunar surface (Halekas et al. 2009a). The authors attributed the low value of the yield to the surface roughness and we are preparing investigations of this effect in the laboratory experiment as well as in simulations.

The work was supported by the Research Plan MSM 0021620860 that is financed by the Ministry of Education of the Czech Republic and partly by the Czech Grant Agency under Contracts 202/08/0063, 202/08/H057, and 209/11/1412. Students M.B. and J.V. thank for support of the Grant Agency of Charles University under Project No. GAUK 171410.

REFERENCES

Abbas, M., Craven, P., Spann, J., West, E., Pratico, J., Tankosic, D., & Venturini, C. 2002, Phys. Scr. T, 98, 99
Abbas, M. M., Craven, P. D., Spann, J. F., West, E., Pratico, J., Tankosic, D., & Venturini, C. C. 2004, ApJ, 614, 781
Abbas, M. M., Tankosic, D., Craven, P. D., LeClair, A. C., & Spann, J. F. 2010, ApJ, 718, 795
Čermák, I. 1994, PhD thesis, Naturwissenschaftlich-Mathematischen Gesamtfakultät, Ruprecht-Karls-Universität, Heidelberg
Čermák, I., Grün, E., & Švestka, J. 1995, Adv. Space Res., 15, 59
Dahneke, B. E. 1973, J. Aerosol Sci., 4, 147
Davis, E. J. 1985, Langmuir, 1, 379
Halekas, J. S., Delory, G. T., Lin, R. P., Stubbs, T. J., & Farrell, W. M. 2008, J. Geophys. Res., 113, A09102
Halekas, J. S., Delory, G. T., Lin, R. P., Stubbs, T. J., & Farrell, W. M. 2009a, Planet. Space Sci., 57, 78
Halekas, J. S., Delory, G. T., Lin, R. P., Stubbs, T. J., & Farrell, W. M. 2009b, J. Geophys. Res., 114, A05110
Halekas, J. S., Lin, R. P., & Mitchell, D. L. 2005, Geophys. Res. Lett., 32, L09102
Halekas, J. S., et al. 2007, Geophys. Res. Lett., 34, L02111
Horanyi, M., & Goertz, C. 1990, ApJ, 361, 155
Horányi, M., Walch, B., Robertson, S., & Alexander, D. 1998, J. Geophys. Res., 103, 8575
Jurac, S., Baragiola, R. A., Johnson, R. E., & Sittler, E. C. 1995, J. Geophys. Res., 100, 14821
Kimura, H., & Mann, I. 1998, ApJ, 499, 454
Loth, E. 2008, Powder Technol., 182, 342
Meyer-Vernet, N. 1982, A&A, 105, 98
Mukai, T. 1981, A&A, 99, 1
Pavlů, J., Němeček, Z., Šafránková, J., & Čermák, I. 2004a, IEEE Trans. Plasma Sci., 32, 607
Pavlů, J., Richterová, I., Němeček, Z., Šafránková, J., & Čermák, I. 2008, Faraday Discuss., 137, 139
Pavlů, J., Šafránková, J., Němeček, Z., & Richterová, I. 2009, Contrib. Plasma Phys., 49, 169
Pavlů, J., Velyhan, A., Richterová, I., Němeček, Z., Šafránková, J., Čermák, I., & Žilavý, P. 2004b, IEEE Trans. Plasma Sci., 32, 704
Richterová, I., Beránek, M., Pavlů, J., Němeček, Z., & Šafránková, J. 2010, Phys. Rev. B, 81, 075406
Richterová, I., Němeček, Z., Šafránková, J., & Pavlů, J. 2004, IEEE Trans. Plasma Sci., 32, 617
Richterová, I., Němeček, Z., Šafránková, J., Pavlů, J., & Beránek, M. 2007, IEEE Trans. Plasma Sci., 35, 286
Richterová, I., Pavlů, J., Němeček, Z., & Šafránková, J. 2006, Phys. Rev. B, 74, 235430
Spann, J., Abbas, M., Venturini, C., & Comfort, R. 2001, Phys. Scr. T, 89, 149
Sternovsky, Z., Horányi, M., & Robertson, S. 2001, J. Vac. Sci. Technol. A, 19, 2533
Stubbs, T. J., Vondrak, R. R., & Farrell, W. M. 2006, Adv. Space Res., 37, 59
Tankosic, D., & Abbas, M. M. 2008, in Lunar and Planetary Institute Science Conference (Lunar and Planetary Science XXXIX) (League City, TX: LPI), 1391
Velyhan, A., Žilavý, P., Pavlů, J., Šafránková, J., & Němeček, Z. 2004, Vacuum, 76, 447
Walch, B., Horanyi, M., & Robertson, S. 1998, in AIP Conf. Proc. 446, Physics of Dusty Plasmas—Seventh Workshop, Boulder, CO, 1998 April, ed. M. Horanyi, S. Robertson, & B. Walch (Melville, NY: AIP), 271
Whipple, E. C. 1981, Rep. Prog. Phys., 44, 1197
Žilavý, P., Sternovský, Z., Čermák, I., Němeček, Z., & Šafránková, J. 1998, Vacuum, 50, 139